



HAL
open science

g-C₃N₄/TiO₂ S-scheme heterojunction photocatalyst with enhanced photocatalytic Carbamazepine degradation and mineralization

Abdoulaye Kane, Latifa Chafiq, Sadou Dalhatou, Pierre Bonnet, Maryline Nasr, Nathalie Gaillard, Jean Marie Dangwang Dikdim, Guillaume Monier, Aymen Assadi, H. Zeghioud

► To cite this version:

Abdoulaye Kane, Latifa Chafiq, Sadou Dalhatou, Pierre Bonnet, Maryline Nasr, et al.. g-C₃N₄/TiO₂ S-scheme heterojunction photocatalyst with enhanced photocatalytic Carbamazepine degradation and mineralization. *Journal of Photochemistry and Photobiology A: Chemistry*, 2022, 430, pp.113971. 10.1016/j.jphotochem.2022.113971 . hal-03655633

HAL Id: hal-03655633

<https://normandie-univ.hal.science/hal-03655633>

Submitted on 29 Apr 2022

HAL is a multi-disciplinary open access archive for the deposit and dissemination of scientific research documents, whether they are published or not. The documents may come from teaching and research institutions in France or abroad, or from public or private research centers.

L'archive ouverte pluridisciplinaire **HAL**, est destinée au dépôt et à la diffusion de documents scientifiques de niveau recherche, publiés ou non, émanant des établissements d'enseignement et de recherche français ou étrangers, des laboratoires publics ou privés.

g-C₃N₄/TiO₂ S-scheme heterojunction photocatalyst with enhanced photocatalytic Carbamazepine degradation and mineralization

Abdoulaye Kane¹, Latifa Chafiq¹, Sadou Dalhatou², Pierre Bonnet³, Maryline Nasr³, Nathalie Gaillard³, Jean Marie Dangwang Dikdim², Guillaume Monier⁴, Aymen Amine Assadi⁵, Hicham Zeghioud^{1*}

¹*UniLaSalle-Ecole des Métiers de l'Environnement, Cyclann, Campus de Ker Lann, 35 170 Bruz, France.*

²*University of Maroua, Faculty of Science, Department of Chemistry, P.O.Box. 814 Maroua, Cameroon*

³*Universite Clermont Auvergne, Institut de Chimie de Clermont-Ferrand (ICCF), 24 Avenue Blaise Pascal, 63178, Aubiere, France*

⁴*Université Clermont Auvergne, CNRS, Clermont Auvergne INP, Institut Pascal, F-63000 Clermont-Ferrand, France*

⁵*Univ. Rennes, Ecole Nationale Supérieure de Chimie de Rennes, CNRS, ISCR, UMR6226, F-3500 Rennes, France.*

* *Corresponding author. E-mail: hicham.zeghioud@unilasalle.fr*

Abstract:

In the present work, UVA light-driven g-C₃N₄/TiO₂ photocatalyst was synthesized for the photodegradation of Carbamazepine (CBZ) in aqueous medium. The morphological, the optical properties and the structure of the TiO₂, g-C₃N₄ and the

prepared composites were analyzed using X-ray diffraction (XRD), Nitrogen adsorption-desorption isotherm based on BET, Raman Spectroscopy, Scanning Electron Microscopy (SEM) with EDX, UV-vis Diffuse Reflectance Spectroscopy (UV-vis DRS). Optical absorption studies revealed a 2.97 and 2.78 eV of band gap for the developed composites for 10%g-C₃N₄/TiO₂ (A10) and 30%g-C₃N₄/TiO₂ (A30), respectively. The N₂ adsorption-desorption isotherm showed an 80.64 and 59.67 m²/g of specific surface area for A10 and A30, respectively. Photodegradation studies show that A10 a composite photo-catalyst can eliminate 71.41% of CBZ with 30.38 % of mineralization yield within 360 min of UVA irradiation at optimum conditions (10 ppm of initial CBZ concentration and 0.1 g of 10%g-C₃N₄/TiO₂ loading). The kinetic results showed that the removal of this pollutant nearly followed a First-order kinetic model with a regression coefficient (R²) values more than 0.98 and a High reaction rate constant recorded of 0.0034 min⁻¹ for A10.

Keywords: photocatalysis, g-C₃N₄/TiO₂, UVA, Carbamazepine, mineralization.

1. Introduction

Hospitals consumed water about 750 liters per bed per day, which is 10 times higher than the daily consumption per citizen. This big consumption implies a significant amount of wastewater. In fact, more than 10% of drug residues found in the surface water in France come from hospitals [1,2]. The specificity of hospital effluents is their complex compositions. They contain 1000 times more detergents than drugs; they also contain pathogenic microorganisms, antibiotic-resistant bacteria, endocrine disruptors, metals, radioisotopes... [3]. Despite their complexity, hospital effluents are considered to be of the same pollutant load as urban wastewaters and are

discharged into public sewer networks [4]. For all these reasons, the development of processes that will allow the pre-treatment of wastewater at health care institutions is necessary in order to reduce the risks of contamination of the public sanitation network, and therefore human and animal health.

Nowadays, Advanced Oxidation Processes (AOP) such as photocatalysis are being studied more and more as a hydrogen production technique [5,6], fuel generation method [7] and alternative methods for the complete elimination of pollution in wastewater, and it's considered one of the most promising green chemistry technologies [8,9]. This process is based on the formation of a strong oxidant; the hydroxyl radical OH° which are characterized by an oxidation potential of +2.80V/ENH [10]. Hence, its high reactivity and its low selectivity allow the mineralization of many organic and inorganic molecules, thus it can ultimately lead to their mineralization, with the formation of CO_2 , H_2O and inorganic ions [10,11].

Titanium dioxide (TiO_2) is the most widely studied, and used for environmental remediation, hydrogen energy production, and solar cells due to its environmental-friendly properties, good chemical stability, high abundance, low cost, and good photocatalytic activity [8,12] Recently, graphite-like carbon nitride has attracted great interest due to its wide potential for photocatalytic application under visible light, owing to its band gap of 2.70 eV, good physicochemical stability, abundance, low cost and can be easily prepared [12,13]. However, many researchers confirm that the photocatalytic performances of TiO_2 and g- C_3N_4 taken separately are still unsatisfying for heterogeneous photocatalysis, Owing to the low solar energy conversion efficiency and the high recombination of photogenerated electron hole pairs [14,15]. In order to overcome the drawbacks of this catalysts many strategies are studied such as doping [14,16], coupling with other semiconductor materials [17,18], the

coupling of the UV and visible light, the addition of strong oxidants such as H_2O_2 , $\text{SO}_4^{\cdot-}$, Fe^{2+} , and O_3 in the reaction medium are used for improving the photocatalytic activity [19,20]. However, coupling two semiconductors to form a heterojunction structure, in other words composite is proven to be a very effective method to improve the photocatalytic efficiency, there are already many researchers focusing on the composite structure of TiO_2 and $\text{g-C}_3\text{N}_4$, and the resultant catalysts prove higher photocatalytic activity [12,21].

The improvement of $\text{g-C}_3\text{N}_4/\text{TiO}_2$ catalyst performance is attributed to the formation of a good heterojunction between the materials leading to a synergetic effect. This includes the increasing of surface area, reduction of band gap, improved charge transfer at the interface as well as the inhibition of their recombination. However, knowing the mechanism involved in the $\text{g-C}_3\text{N}_4/\text{TiO}_2$ heterostructure is very important to explain the enhancement of the catalytic efficiency. Several techniques were employed for this purpose including quenching tests, electron paramagnetic resonance (EPR) analyses, spectroscopic analyses (XPS) and density functional theory (DFT) calculations. The combination of these methods has significantly contributed on identification of the real type of constructed heterostructure. For many years, the mechanisms of charge transfer were mainly explained by II-type heterojunction and Z-scheme [22,23].

Unfortunately, these mechanisms presented some limitations from thermodynamically and kinetically plans particularly, thus reduce both oxidant and reductant power of the photocatalyst [24,25]. Consequently, a new heterojunction called step-scheme "s-scheme" has been recently proposed by Fu et al. (2019) research group to overcome these drawbacks [25]. In this mechanism, not only the

migration of electrons is accelerated, but their reduction performance is effectively exploited [26].

Briefly, S-scheme heterojunction involves two n-type semiconductors where the one with high conduction band (CB) energy is considered as reduction photocatalyst and the other as oxidation photocatalyst [27]. When irradiated, the electrons in the CB of OP were moved to VB of RP for recombination. Meanwhile, both endowed with high redox potential, electrons accumulated in CB of RP and holes contained in VB of OP were largely available for redox reactions [24,28]. As a result, recent advances on designing g-C₃N₄ heterostructures based on s-scheme mechanism have significantly contributed to the improvement of photocatalytic degradation of pollutants [29-33].

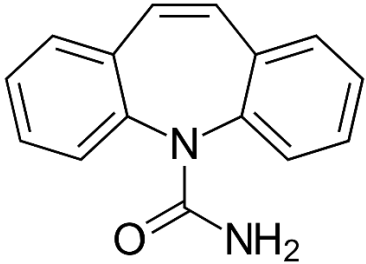
In this present paper we report the elaboration of g-C₃N₄/TiO₂ composites with different amount of g-C₃N₄ and starting from the synthesis of basic materials based on ecological criterion. The photocatalytic performance of as-prepared materials was evaluated through the photodegradation of Carbamazepine under UVA. The degradation mechanism was also discussed. We choose to study the degradation of Carbamazepine because it's one of the most frequently used drugs for the treatment of epilepsy, bipolar disorder and as mood stabilizing [34]. The large-scale use and its resistance to conventional and biological water treatment explain its presence and its persistence in the surface waters, furthermore CBZ is categorized as toxic to aquatic life including bacteria, invertebrates, algae and fish [19, 35].

2. Experiment

2.1. Chemical reagents

Titanium isopropoxyde (TTiP, 99%) was purchased from Sigma Aldrich, acetic acid (CH₃COOH), dicyandiamide (C₂H₄N₄), methanol (CH₃OH) and carbamazepine (C₁₅H₁₂N₂O) were purchased from VWR. All reagents were of analytical grade and were used without further purification. Ultra-pure water was used throughout the experiments carried out in this study to avoid any external contamination. The physicochemical properties of CBZ are presented in table 1.

Table 1: Physicochemical properties of CBZ.

Propriety	Carbamazepine
Empirical formula	C ₁₅ H ₁₂ N ₂ O
Molecular weight (g/mol)	236,27 g/mol
Abbreviation	CBZ
λ_{\max} (nm)	265 nm
Chemical structure	

2.2. Synthesis: Catalyst preparation

2.2.1. Synthesis of titanium dioxide (TiO₂)

The TiO₂ nanoparticles were prepared by the sol-gel method, based on the previous literature [17]. Typically, 20 mL of titanium isopropoxide were dissolved in 40 mL of acetic acid. To homogenize, the solution was set under constant stirring for 15 min, the hydrolysis was accomplished by adding 120 mL of deionized water drop by drop, and then the solution was maintained under stirring for 2 h. Afterwards, the gel was placed in the oven at 90°C for 12 h. Sallow-white crystals were obtained by drying the gel at 200°C for 2 h. The sample was pulverized in a porcelain mortar, and then annealed in air at 400 °C for 4 h.

2.2.2. Synthesis of graphitic carbon nitride (g-C₃N₄)

The bulk g-C₃N₄ was prepared by thermal polymerization based on previous literature [2,3]. Typically, 10 g of dicyandiamide was put into an alumina crucible, and then it was heated at 550°C in a muffle furnace for 4 hours at a heating rate of 20°C/min. After cooled to room temperature, the yellow sample was pulverized into powders for further use.

2.2.3. Synthesis of g-C₃N₄/TiO₂ composite

The g-C₃N₄/TiO₂ composite were achieved by wet-impregnation method [8]. In a typical procedure, the appropriate amount of g-C₃N₄ and TiO₂ were dissolved separately by methanol in beakers. Then, the beakers were placed in an ultrasonic bath for 30 min. Then the two solutions were mixed and stirred at room temperature for 24 h. The resulting powder was maintained under room temperature for 12 h to evaporate the solvent. The obtained photocatalysts were denoted as X %CN/TO (X is the g-C₃N₄ percentage mass ratio).

The photo-catalytic treatment setup (Figure 1S), its description and experimental conditions were reported in detail in supporting information.

2.3. Sample characterization

- The X-ray diffraction (XRD) patterns of as-prepared catalysts were made using a D8 Bruker spectrometer with $\lambda=0.15418$ nm as a wavelength of the beam, the incident angle of 2θ , 5-130° using 0,017° each step, and the acceleration tension is 40 kV and current emission equals 30 Ma.

- Nitrogen adsorption-desorption isotherm were obtained using a Quantachrome instrument at 77k. The specific surface area measures are based on Brunauer-Emmett-Teller's equation (BET).

- Raman spectra were acquired by using Raman spectrometer of JobinYvon company model T64000. The wavelength of laser was 514.5 nm (2.41 eV) and the power was set at 100 mWatt. The measurement was carried out in solid state by dispersing the sample powder upon glass slide under air at room temperature.

- The scanning electron microscopy (SEM) images of the photocatalysts were obtained using an (JEOL 5910 LV) apparatus with EDS elementary analysis using SDD detector (Bruker)

- The UV-vis diffuse reflectance spectra (UV-vis DRS) of the photocatalysts were recorded by Cary 300 instrument with scan Rate of 600 (nm/min) in shifting range of 80 to 500 cm^{-1} .

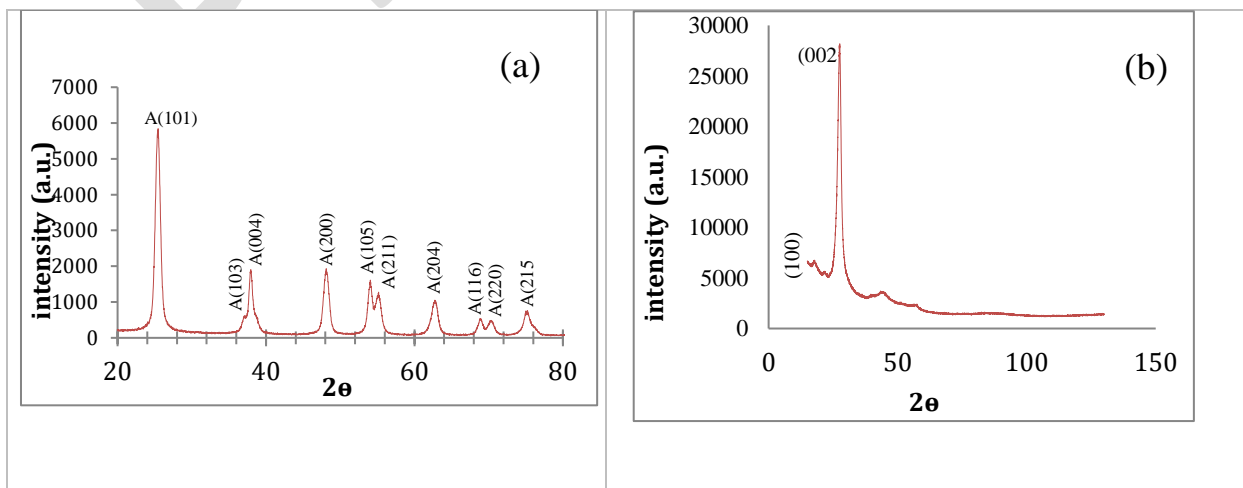
- The chemical states of wt%g-C₃N₄/TiO₂ composites were analyzed using X-ray photoelectron spectroscopy (XPS) in an ultrahigh vacuum photoelectron spectrometer equipped with an Omicron DAR 400 X-ray source (Mg K α source at 1253.6 eV) and an Omicron EA 125 hemispherical analyzer.

3. Results and discussion

3.1. Crystal structure

The XRD patterns of the prepared samples are shown in Fig.1. For TiO₂ (figure 1a), the diffraction picks are : $2\theta = 25,32^\circ, 37,82^\circ, 47,07^\circ, 53,97^\circ, 55,15^\circ, 62,75^\circ, 68,72^\circ, 70,30^\circ$ and $75,12^\circ$ the projections of these values on a crystallographic plane gives the following (hkl) coordinates : (101), (004), (200), (105), (211), (204), (116), (220) and (215). Based on these results we conclude that the crystallographic plane corresponds to Anatase phase (JCPDS 21-1272), which confirms that our TiO₂ is mostly Anatase [36]. The g-C₃N₄ analysis results (figure 1b), shows that the compound is pure with a pic at $2\theta = 13,1^\circ$ that corresponds to the plan (100) of tri-s-triazine, and the pic at $27,4^\circ$ relative to crystallographic plane (002) which is generated by an inter-layer stack [37,38].

Regarding to composite materials (fig.1c), we notice that TiO₂ and g-C₃N₄ coexist in composites, the peaks appeared on the XRD patterns of both g-C₃N₄ and TiO₂ can be observed without obvious change. The effect of thermal treatment of g-C₃N₄ under Argon was also discussed in fig 2S and 3S.



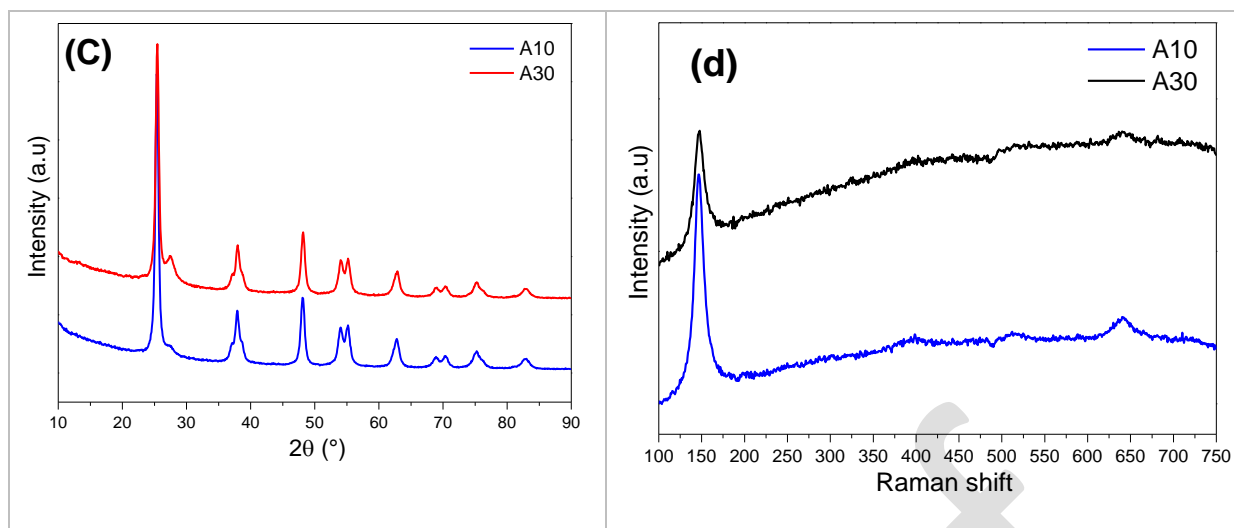


Figure 1: DRX of; (a) TiO_2 with A for Anatase (b); $\text{g-C}_3\text{N}_4$, (c) the composite wt% $\text{g-C}_3\text{N}_4/\text{TiO}_2$ and (d) Raman spectra of wt% $\text{g-C}_3\text{N}_4/\text{TiO}_2$

The crystallinity of the composites 10% and 30% of $\text{g-C}_3\text{N}_4$ was measured by Raman spectroscopy (Fig. 1d). The figures display the presence of TiO_2 anatase phase, which is correlated with diffraction analysis (*The main bands of interest are 143 cm^{-1} , 195 cm^{-1} , 395 cm^{-1} , 515 cm^{-1} , and 640 cm^{-1}*) [39], while the $\text{g-C}_3\text{N}_4$ does not appear on the Raman spectrum because of its fluorescence.

3.2. Specific Surface Area (SSA)

The N_2 adsorption-desorption isotherm of TiO_2 , $\text{g-C}_3\text{N}_4$, A10 and A30 are shown in table 2. According to the Brunauer-Emmett-Teller (BET) theory, pure TiO_2 had a high surface area of $125.57 \text{ m}^2/\text{g}$, while $\text{g-C}_3\text{N}_4$ had a relatively low surface area of $10.51 \text{ m}^2/\text{g}$. This means that the elaborated TiO_2 would be able to better fix the molecule to be degraded than $\text{g-C}_3\text{N}_4$. Moreover, the initial surface area of TiO_2 gradually diminish as carbon nitride presence rises, the value goes from $80.65 \text{ m}^2/\text{g}$ to $59.67 \text{ m}^2/\text{g}$ for 10% and 30% of carbon nitride respectively. This is due to the effect of the incorporation of the carbon nitride into the TiO_2 pores.

Table 2: The specific surface area of the samples

Materials	g-C ₃ N ₄	TiO ₂	A10	A30
Specific surface area (m ² /g)	10.51	125.57	80.65	59.67

3.3. Morphology and elemental analysis

The morphology and microstructure of as-prepared samples were further investigated by SEM images (Fig. 2). The SEM studies of the composite 10%wt of carbon nitride (Fig. 3a) showed agglomerated TiO₂ nanoparticles attached on to the sheet-like structure of g-C₃N₄. Thus, we can conclude that the composite A10 present a good homogeneity. From Fig. 3c, it can be seen that the composite with 30%wt of carbon nitride present less good homogeneity comparing to A10, but still have a good morphology, and A30 could present a good ability to ensure a good separation of the charges. Thus, this will allow decreasing the rate of recombination.

Moreover, the EDX analysis clearly confirms, the purity of the all our samples and also confirms the presence of g-C₃N₄ in lower amount with respect to TiO₂ in both composites. The good homogeneity between TiO₂ and g-C₃N₄ should facilitate the efficient removal of photo-generated electrons accumulate on (101) facets of TiO₂, leaving holes left on (001) facets. This efficient special separation of photo-generated electron-hole pairs in the composite should benefit the photocatalytic activity.¹

¹ Effect of contact interface between TiO₂ and g-C₃N₄ on the photoreactivity of g-C₃N₄/TiO₂ photocatalyst: (0 0 1) vs (1 0 1) facets of TiO₂.

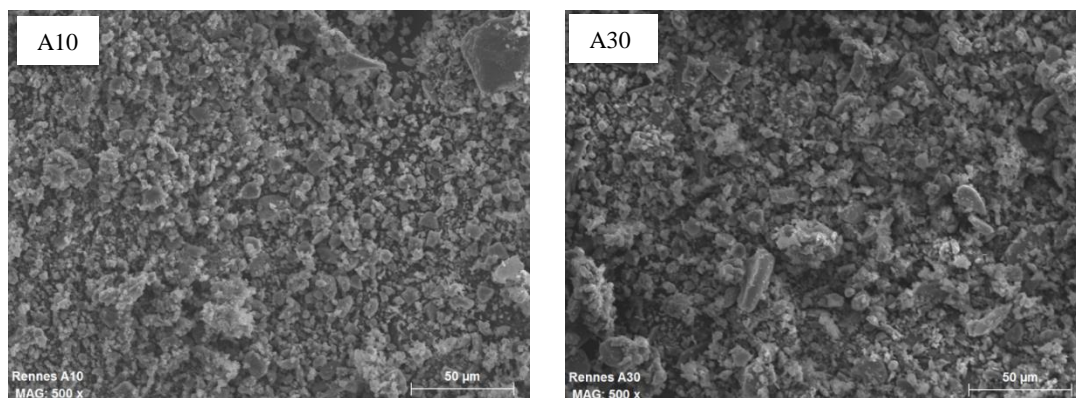


Figure 2: SEM images of A10 and A30

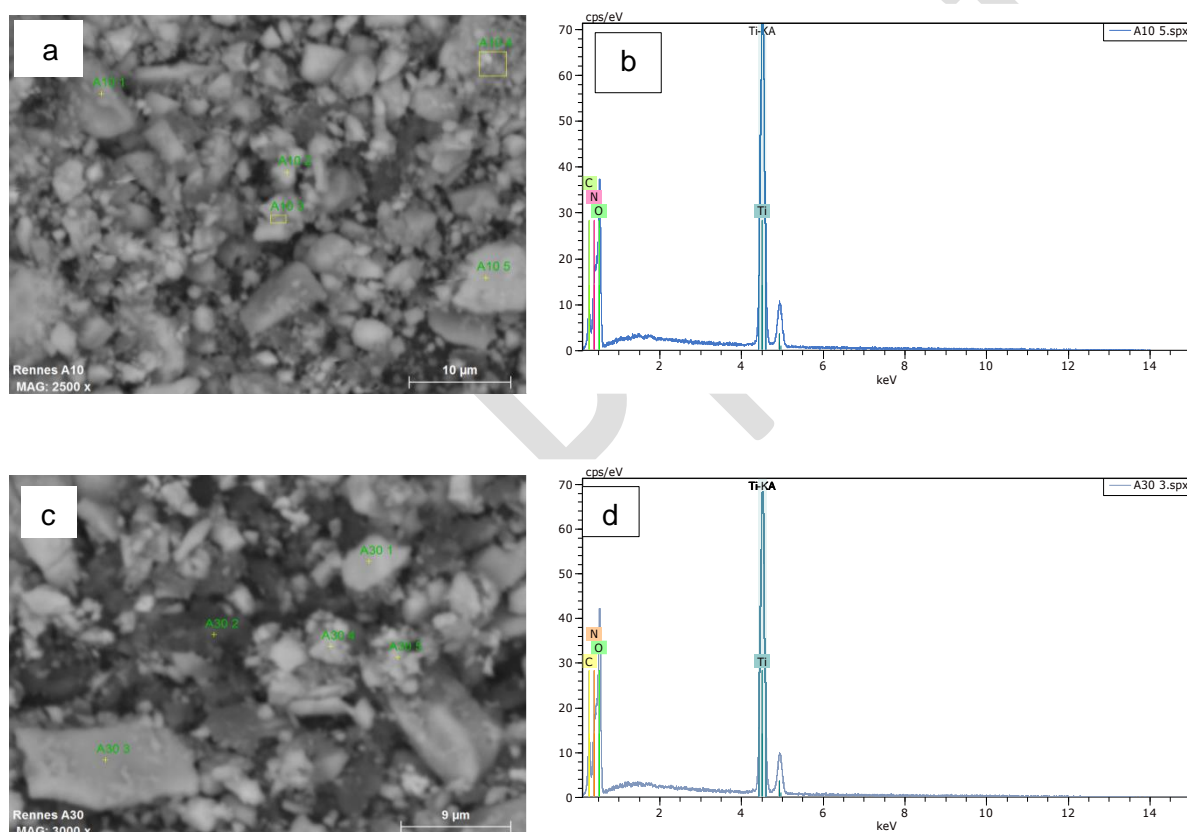
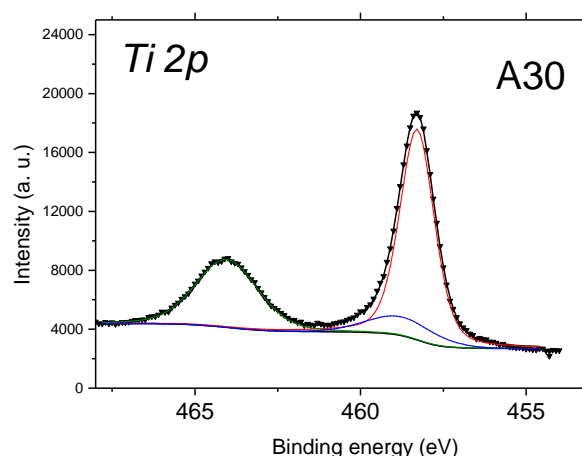
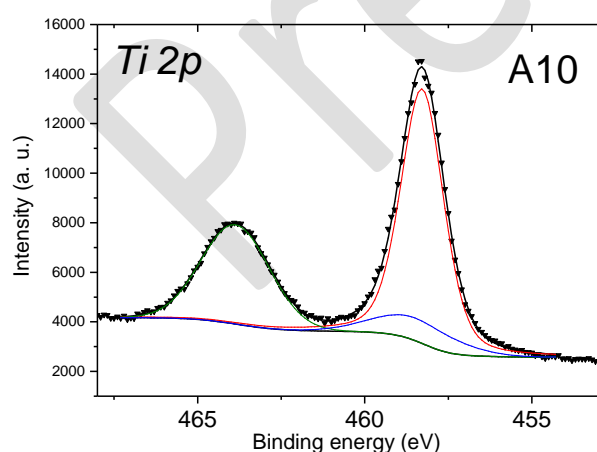
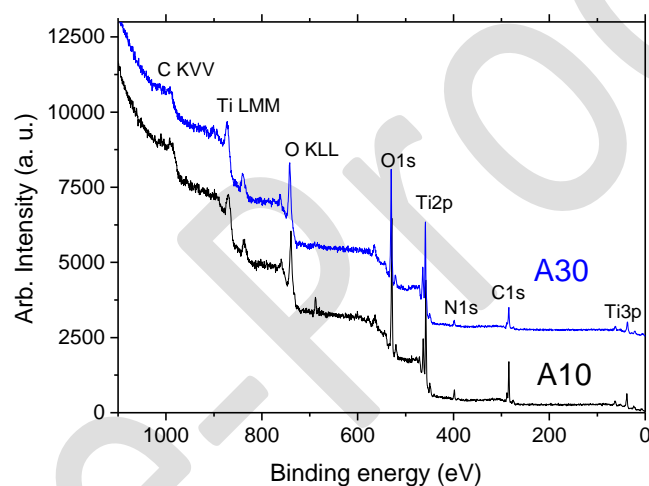


Figure 3: SEM images with EDX spectra respectively (a) & (b) for A10; (c) & (d) for A30.

The XPS spectra of the Ti 2p, C 1s, O1s and N1s core levels are presented in Fig. 4 for A10 and A30. Slight differences between the two wt%g-C₃N₄/TiO₂ composite spectra are detected. For A30, a pure TiO₂ phase is shown by the Ti2p (Ti2p_{3/2} at 458.3 eV) and O1s peak decompositions, and the gC₃N₄ phase is observed in the

C1s (N-C=N at 288.5 eV) and N1s (C-N=C at 398.4 eV) peak decompositions [40]. These results point out the fact that there are very weak interactions between the TiO₂ and the gC₃N₄ particles. For A10, the TiO₂ phase is also revealed in the Ti2p and O1s peak decompositions but a slight widening of the Ti2p peak is observed which may be due to the formation of Ti³⁺ or to the possible interaction with gC₃N₄. This last interpretation is strengthened by the energy shift observed in the C1s (N-C=N at 289.7 eV) and N1s (C-N=C at 397.8 eV) peaks. Moreover, the XPS results are consistent with EDX analysis showing no contamination.



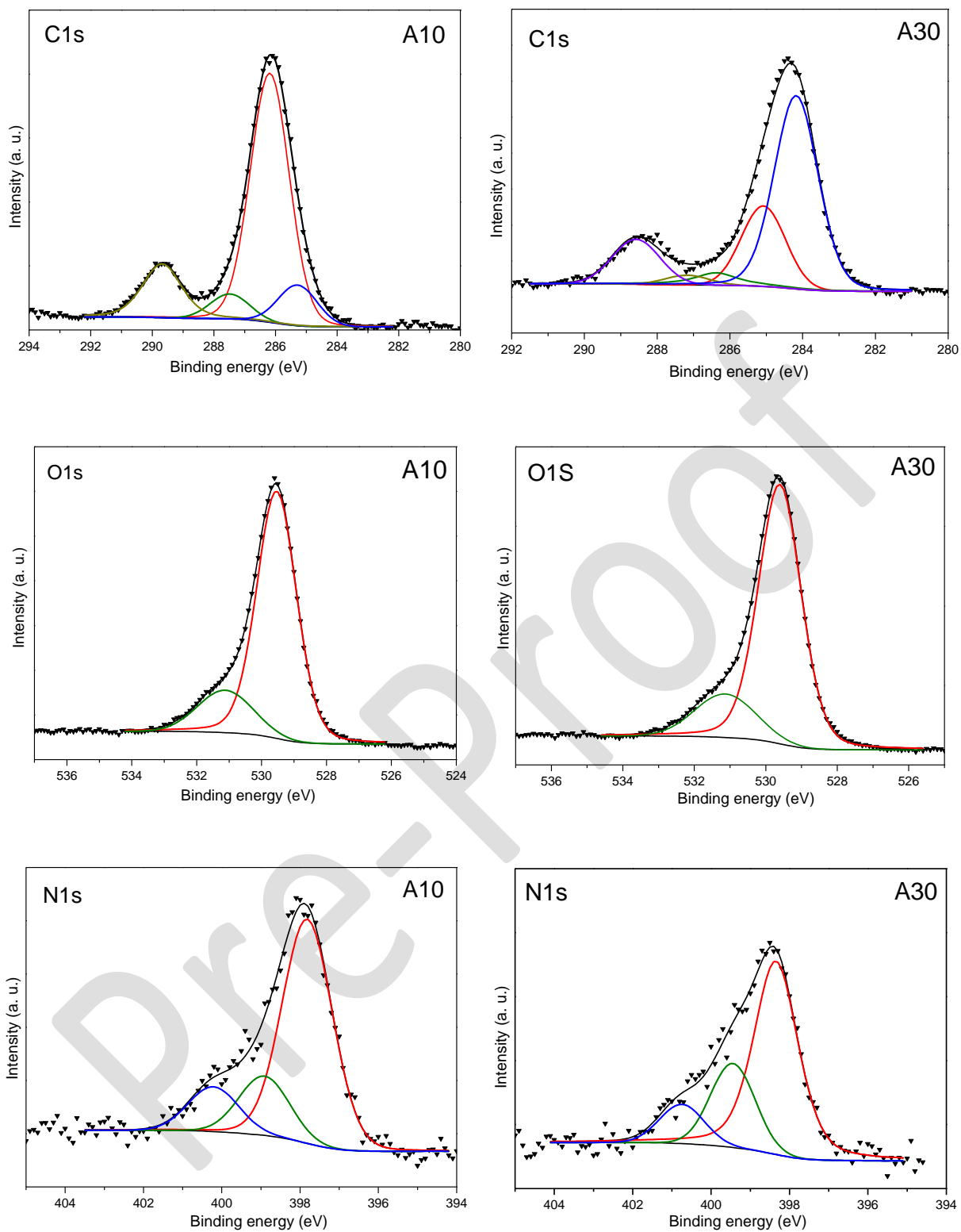


Figure 4: the XPS spectra for A10 and A30.

3.4. Optical absorption studies (UV-vis Diffuse Reflectance)

We carried out the diffuse spectral analysis (DRS) of the calcined TiO_2 , the pure $\text{g-C}_3\text{N}_4$ and the two composite A10 and A30, in order to study the absorption spectra and the change of the band gap of our samples caused by the heat treatment and the addition of 10 and 30%wt of $\text{g-C}_3\text{N}_4$. According to the obtained results of the DRS as displayed in Fig. 5 (a) the absorption sharp edges of TiO_2 , the pure $\text{g-C}_3\text{N}_4$ and the two composites A10 and A30 were found to be around 399.11, 459.72, 446.5, 415.13 nm respectively. Moreover, the band gap values (E_g) of TiO_2 , the pure $\text{g-C}_3\text{N}_4$ and the two composites A10 and A30 were calculated as 3.11, 2.7, 2.99, and 2.78 eV, respectively. Similar results for $\text{g-C}_3\text{N}_4$ ($E_g= 2.84$ eV) are reported by Liao et al [41]. It is obvious that the TiO_2 and the two composites will absorb in visible region, the band gap was decreased because of the addition of the $\text{g-C}_3\text{N}_4$ and because of the creation of the oxygen vacancies due to the thermal treatment. Indeed, comparing to the pure TiO_2 , the composites exhibited enhanced absorption at higher wavelengths due to the optimal heterojunction created between the two basic materials.

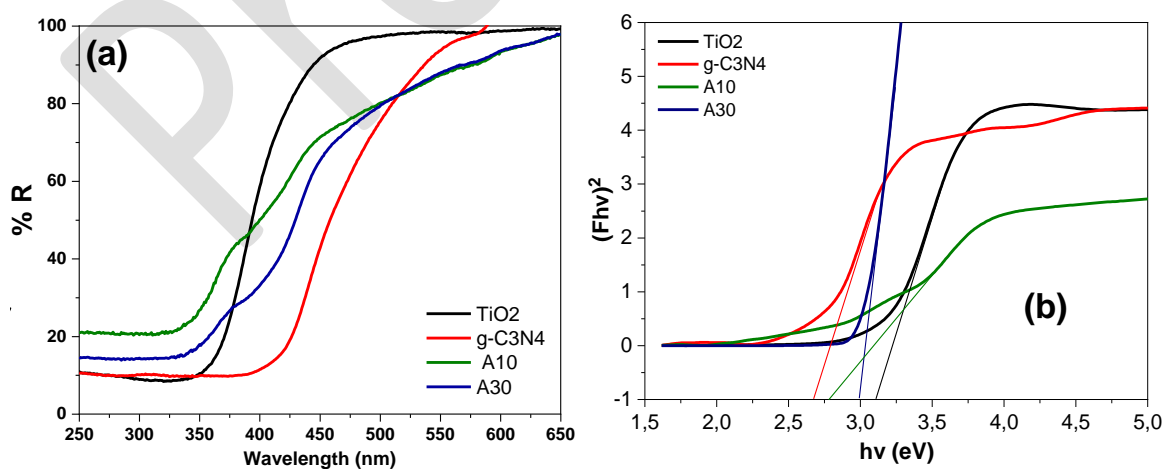


Figure 5: (a) Diffuse Reflectance Spectra of pure $\text{g-C}_3\text{N}_4$, TiO_2 and the two composites $\text{g-C}_3\text{N}_4/\text{TiO}_2$ of 10 and 30% of $\text{g-C}_3\text{N}_4$. (b) Plot of transferred Kubelka-

Munk versus energy of the light absorbed of pure $g\text{-C}_3\text{N}_4$, TiO_2 , and the tow composites $g\text{-C}_3\text{N}_4/\text{TiO}_2$ of 10 and 30% of $g\text{-C}_3\text{N}_4$.

3.5. Evaluation of photocatalytic activity of samples

3.5.1. Photocatalytic tests

The effect of photolysis on CBZ degradation (fig 4S) and the photocatalytic activities of TiO_2 , $g\text{-C}_3\text{N}_4$ and the as prepared catalytic composites samples were firstly tested for CBZ degradation (Fig 5S and 6S). The results are summarized and presented at the Fig 6(a).

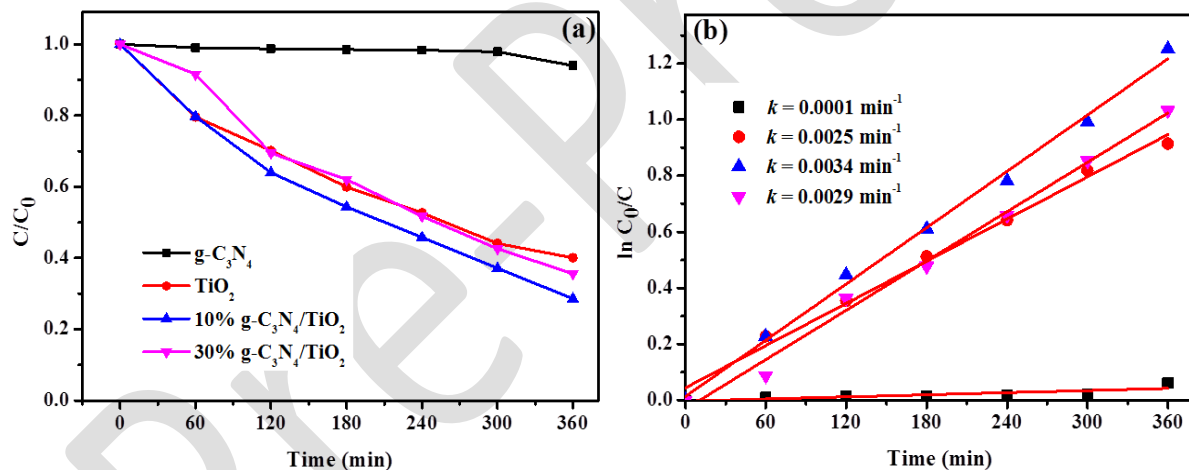


Figure 6: (a) Degradation of CBZ by photocatalysis under UV irradiation, (b) First-order kinetic modelling. Conditions: CBZ: 10 mg/L, Catalyst: 0.1 g, $\lambda = 285 \text{ nm}$.

From Fig 6(a), it can be seen that the doping of TiO_2 increase the CBZ removal. After 6 h of UV light irradiation, the degradation percentages were 5.97, 59.94, 71.41 and 64.39% for $g\text{-C}_3\text{N}_4$, TiO_2 , 10% $g\text{-C}_3\text{N}_4/\text{TiO}_2$ and 30% $g\text{-C}_3\text{N}_4/\text{TiO}_2$, respectively. It is obvious $g\text{-C}_3\text{N}_4$ exhibited the lowest photocatalytic effect. This is because of its poor

photo-response under UV area. The 10% g-C₃N₄/TiO₂ sample shows the best catalytic performance because of the low band gap values (2.78 eV) compared to the other materials (TiO₂ (3.11 eV) and 30% g-C₃N₄/TiO₂, (2.99 eV)) evaluated from Diffuse Reflectance Spectra, which can lead to an enhancement of the absorption of UV light. Both composite materials possess higher degradation activity than pure TiO₂, which highlight the synergetic effect between the two raw materials through the electron-hole separation [42,43]. In addition, the performance of composite material revealed that A10 is better than A30, meaning an optimal value of g-C₃N₄ loading is 10%. This behavior could be explained by two reasons: in one hand, the loading of excess amount of g-C₃N₄ particles in TiO₂ may reduce the availability of catalytic sites for CBZ degradation by a formation of a barrier layer coating the surface of TiO₂ [44]. This clearly is in consistent with the less homogeneity structure of A30 compare to A10 observed in SEM images (Fig 2) as well as the BET surface area of the samples (Table 2). Secondly, the superior light absorption for A30 means it could be more sensitive in higher wavelengths according to UV-Vis absorption spectra and then it might be have good catalytic activity in this light area compare to the one used in this study.

The kinetic degradation of CBZ has been checked according to the first-order model which the equation (1) is expressed below:

$$\ln \frac{C}{C_0} = -kt \quad (1)$$

Where: C_0 and C are the initial concentration of CBZ and after a given treatment time. k is the apparent rate constant (min^{-1}) and t the time (min).

The Fig 6(b) illustrates the plot of $\ln C_0/C$ vs t . It could be observed that the degradation of CBZ by g-C₃N₄/TiO₂ composite fits well the pseudo-first order model which can be explained by the straight line and good regression coefficient ($R^2 >$

0.98). Such as for the degradation percentage, the reaction rate is fastest in the case of A10 material ($k=0.0034 \text{ min}^{-1}$) compare to the other materials. The apparent kinetics constants were 0.0025 min^{-1} and 0.0029 min^{-1} for A30 and pure TiO_2 , respectively. This finding indicates that the photocatalytic performance has been promoted through the loading of g- C_3N_4 onto TiO_2 .

The present results are compared with those reported in literature (Table 3). Even some works reported relatively higher photodegradation with less time taken for the photocatalytic treatment, the initial concentration of Carbamazepine treated in the present study is relatively higher than those reported in some studies. The developed catalyst presented a good specific area and an interesting band gap.

Table 3: Comparison of present degradation efficiency with literature data.

Photocatalyst	Bande Gap (eV)	Surface area (SBET) (m^2/g)	Pollutant (Initial.con)	Treatment duration	Degradation efficiency	Referenc es
g- $\text{C}_3\text{N}_4/\text{TiO}_2$ (1:4)	2.8	176	-	-	-	[45]
g- $\text{C}_3\text{N}_4/\text{TiO}_2$	2.83	70.2	Rhodium Boride (4.79 mg/l)	80 min	100 %	[46]
g- $\text{C}_3\text{N}_4/\text{TiO}_2$	-	-	Methyl orange (5 mg/l)	180 min	80.33 %	[47]
g- $\text{C}_3\text{N}_4/\text{TiO}_2$ nanotube	-	-	2-Chlorophen (30 mg/l)	180 min	96.6%	[48]

TiO ₂ @g-C ₃ N ₄	2.97	155	Indigo Carmine (25 mg/l)	60 min	100 %	[49]
TiO ₂ /g-C ₃ N ₄	3.05	14.44	Diclofenac (5 mg/l)	90 min	93.5%	[50]
g-C ₃ N ₄ /TiO ₂	2.99	80.647	Carbamazepine (10 mg/l)	360 min	71,41%	Present Study

The effect of some operating parameters such as calcination of catalyst and H₂O₂ addition on the photo-catalytic degradation of CBZ was also investigated and discussed in the supporting information (Fig 7S).

3.5.2. Mechanism of CBZ degradation

For better understanding the mechanism of the augmentation of the degradation efficiency by 10% g-C₃N₄/TiO₂ composite material, the charge separation at the interface of the two semi-conductors was investigated and the possible degradation mechanism of CBZ under 10% g-C₃N₄/TiO₂/UV system was illustrated in Fig 7.

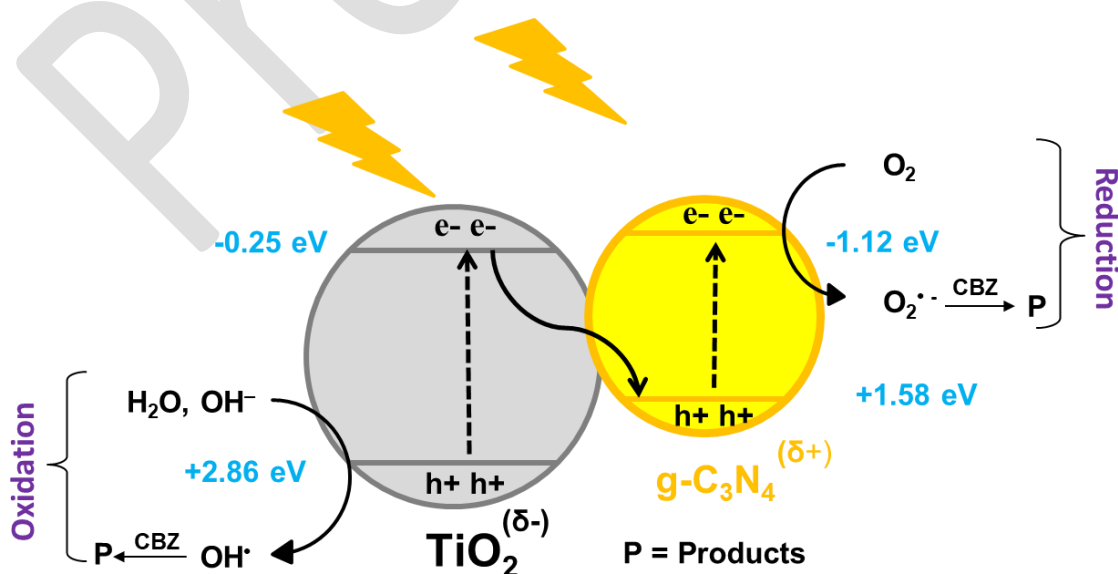


Figure 7: Possible mechanism of g-C₃N₄/TiO₂ heterostructure under UV irradiation

The conduction (E_{CB}) and valence (E_{VB}) bands energy were calculated through the following equation 2 and 3 [51]:

$$E_{CB} = \chi - E^0 - \frac{1}{2}E_g \quad (2)$$

$$E_g = E_{VB} - E_{CB} \quad (3)$$

Where: χ is the electronegativity of the semiconductor and the value were 4.73 and 5.81eV for g-C₃N₄ and TiO₂, respectively [52]. E^0 is the energy of free electrons vs NHE (4.5 eV) [53]. From UV-Vis absorption spectra the band gap energy (E_g) obtained in this study were 3.11 and 2.7 eV for pure TiO₂ and g-C₃N₄, respectively. Then, the E_{CB} and E_{VB} were calculated and the values were of -0.25 and +2.86 eV for TiO₂, whereas the values were -1.12 and +1.58 eV for g-C₃N₄.

Additionally, it is widely reported that the energy level of Fermi for pure TiO₂ is less than pure g-C₃N₄ [54,55]. However, when they are in contact such as the present case, the electrons migrate continuously from g-C₃N₄ to TiO₂ up to reaching the same Fermi energy. As a result, those movements of electrons provoke the upward and downward band edge of TiO₂ and g-C₃N₄, respectively. This migration of electron also leads to the creation of partial charges on each semiconductor and a built of an internal electric field with TiO₂ positively charged whereas g-C₃N₄ is negatively charged. The obtained E_{CB} value of TiO₂ (-0.25 eV) superior than redox potential of O₂/O₂^{•-} (-0.33 V vs. NHE, pH = 7) [32], obviously suppose that reaction of reduction of adsorbed O₂ to form O₂^{•-} cannot occur on CB of TiO₂. In the same way, the H₂O oxidation to form HO[•] at g-C₃N₄ VB could not be possible due to fact that the

E_{VB} value (+1.58 eV) is less positive than potential of HO•/H₂O (2.27 V vs. NHE, pH = 7) [56]. Consequently, the charge migration exhibited in this work obeys also to the typical S-scheme heterojunction mechanism [27,29-30,33]. The photocatalytic mechanism of CBZ degradation could be explained as follows: when the composite material is irradiated by UV light, the electrons were moved from VB to CB of TiO₂^(δ-). Subsequently, these electrons were transferred to the VB of g-C₃N₄^(δ+) for recombination with holes. Therefore, free electrons in CB of g-C₃N₄ and holes in VB of TiO₂ were effectively used in oxidizing reactions for CBZ removal while owing in the same time the long life of useful photo-generated species. This inhibition of electron-holes pair recombination in this S-scheme heterojunction is responsible in the improvement of photocatalytic activity.

3.5.3. Mineralization studies

In order to test the catalytic ability of the composite for mineralization of CBZ, the total organic carbon (TOC) has been measured after 6 h of irradiation. The result is displayed at the Fig 8.

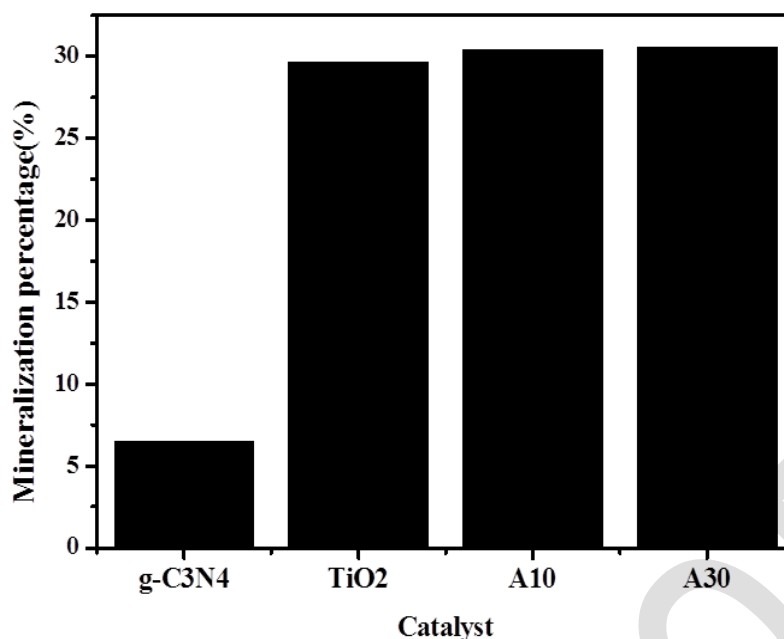


Figure 8: Mineralization of CBZ by photocatalysis under UV irradiation. Conditions:

CBZ: 10 mg/L, Catalyst: 0.1 g, $\lambda = 285$ nm.

From Fig 8, the mineralization percentages were 29.64, 30.38 and 30.54% for pure TiO₂, A10 and A30, respectively. The trend of catalytic activity for destruction of total organic pollution was quite same for the new composite materials prepared in this study. This result revealed also the good performance of A10 and A30 for mineralization of CBZ in water environment.

It is to be noticed that the degradation efficiency for all photocatalytic samples are higher than the mineralization efficiency, it seems that the generated reactive oxygen species (ROS) destroyed in the first step the target molecules until certain degradation percentage and then mineralized the obtained intermediate products, as a second step, similar results were reported in the works of Zeghioud et al. (2019) and Sirtori et al. (2009) [57,58].

4. Conclusion

The new catalytic materials g-C₃N₄/TiO₂ were prepared by wet-impregnation method. Different amounts of g-C₃N₄ were successfully loaded onto TiO₂ according to the characterization analyses. The thermal treatment contributes to create the oxygen vacancies. The A10 material showed well distribution of g-C₃N₄ on TiO₂ and the morphology reveals a quite homogeneity structure. The materials were tested for the photodegradation of CBZ under UV irradiation. The 10% g-C₃N₄/TiO₂ showed remarkable catalytic activity with the best degradation percentage of 71.41% and the highest reaction rate (0.0035 min⁻¹). The enhancement of catalytic efficiency of the composite was attributed to the good heterojunction between the two semiconductors leading to a synergetic effect. This, through an increasing of the surface area, diminution of band gap and the efficient electron-hole pairs separation. This study demonstrates an efficient approach to improve the performance of heterogeneous photocatalysis applied in the field of wastewater treatment.

Acknowledgments

The authors would like to thank Ivane LELIEVRE (Unilasalle Rennes) for her technical help and Lawrence Frezet for BET measurements (ICCF). The authors also thank the Labex IMOBS3 for the financial support (Maryline NASR grant for N-MAFEN² project).

References

- [1] C. Brunel, A.-M. Crignon, P. Feldman, M. Godard, V. Gourdet, A. Harel, M. Hofman, M. Lerouge, A. Paquette, T. Soulet, S. Vassal, V. Yakar, Elimination des effluents liquides des établissements hospitaliers. Rapport CLIN, *Cpias*, (1999) 1–74.
- [2] E. Emmanuel, Evaluation Des Risques Sanitaires Ecotoxicologiques Liés Aux Effluents Hospitaliers, (2004).
- [3] R. H. C. Dremont, “La Gestion des Effluents Liquides en Milieu Hospitalier,” 1997. [Online]. Available: http://www.utc.fr/~mastermq/public/publications/qualite_et_biomedical/UTC/des_s_tbh/96-97/Projets/EL/EL.htm. [Accessed: 10-May-2018].
- [4] P. Verlicchi, A. Galletti, M. Petrovic, and D. BarcelÓ, Hospital effluents as a source of emerging pollutants: An overview of micropollutants and sustainable treatment options, *J. Hydrol.*, 389 (3–4) (2010) 416–428.
- [5] J. Jiang, G. Wang, Y. Shao, J. Wang, S. Zhou, Y. Su, Step-scheme ZnO@ZnS hollow microspheres for improved photocatalytic H₂ production performance, *Chinese Journal of Catalysis* 43 (2022) 329–338.
- [6] Y.-W. Liao, J. Yang, G.-H. Wang, J. Wang, K. Wang, S.-D. Yan, Hierarchical porous NiO as a noble-metal-free cocatalyst for enhanced photocatalytic H₂ production of nitrogen-deficient g-C₃N₄, *Rare Met.* <https://doi.org/10.1007/s12598-021-01784-3>.
- [7] K. Wang, H. Wang, Q. Cheng, C. Gao, G. Wang, X. Wu, Molecular-functionalized engineering of porous carbon nitride nanosheets for wide-spectrum responsive solar fuel generation, *Journal of Colloid and Interface Science* 607 (2022) 1061–1070.

- [8] R. A. Senthil, J. Theerthagiri, A. Selvi, and J. Madhavan, Synthesis and characterization of low-cost g-C₃N₄/TiO₂ composite with enhanced photocatalytic performance under visible-light irradiation, *Opt. Mater. (Amst)*., 64 (2017) 533–539.
- [9] C. Miranda, H. Mansilla, J. Yanez, S. Obregon, and G. Colon, Improved photocatalytic activity of g-C₃N₄/TiO₂ composites prepared by a simple impregnation method, *J. Photochem. Photobiol. A Chem.*, 253 (2013) 16–21.
- [10] G. Carre, Compréhension des mécanismes lors de la photocatalyse appliquée à la dégradation des microorganismes. Application au traitement de l'air et aux textiles auto-décontaminants, (2013).
- [11] F. Zaviska, P. Drogui, G. Mercier, and J.-F. Blais, Procédés d'oxydation avancée dans le traitement des eaux et des effluents industriels: Application à la dégradation des polluants réfractaires, *Rev. des Sci. l'eau*, 22 (4) (2009) 535.
- [12] Y. Jiang, F. Li, Y. Liu, Y. Hong, P. Liu, and L. Ni, "Construction of TiO₂ hollow nanosphere/g-C₃N₄ composites with superior visible-light photocatalytic activity and mechanism insight, *J. Ind. Eng. Chem.*, 41 (2016) 130–140.
- [13] A. Wang, C. Wang, L. Fu, and W. W. Yucheng, Recent Advances of Graphitic Carbon Nitride-Based Structures and Applications in Catalyst, Sensing, Imaging, and LEDs, 9:47 (2017) 1-21.
- [14] H. W. Jiang, Longbo, Xingzhon Yuan, Yang Pan, Jie Liang, Guangming Zeng, Zhibin Wu, Doping of graphitic carbon nitride for photocatalysis: A review, *Elsevier*, 217 (2017) 388-406.

- [15] R. Camposeco, S. Castillo, J. Navarrete, and R. Gomez, Synthesis, characterization and photocatalytic activity of TiO₂ nanostructures: Nanotubes, nanofibers, nanowires and nanoparticles, *Catal. Today*, 266 (2016) 90–101.
- [16] S.F. Chen, J.P. Li, K. Qian, W.P. Xu, Y. Lu, W.X. Huang, S. H. Yu, Large scale photochemical synthesis of M@TiO₂ nanocomposites (M = Ag, Pd, Au, Pt) and their optical properties, CO oxidation performance, and antibacterial effect,” *Nano Res.*, 3(4) (2010) 244–255.
- [17] M. B. Askari, Z. Tavakoli Banizi, M. Seifi, S. Bagheri Dehaghi, and P. Veisi, Synthesis of TiO₂ nanoparticles and decorated multi-wall carbon nanotube (MWCNT) with anatase TiO₂ nanoparticles and study of optical properties and structural characterization of TiO₂/MWCNT nanocomposite, *Optik (Stuttg.)*, 149, (2017) 447–454.
- [18] S. Zarrin, F. Heshmatpour, Photocatalytic activity of TiO₂/Nb₂O₅/PANI and TiO₂/Nb₂O₅/RGO as new nanocomposites for degradation of organic pollutants, *J. Hazard. Mater.*, 351 (2018)147–159.
- [19] F. Ali, J. A. Khan, N. S. Shah, M. Sayed, and H. M. Khan, Carbamazepine Degradation by UV and UV-assisted AOPs: Kinetics, Mechanism and Toxicity Investigations, *Process Saf. Environ. Prot.*, 117 (2018) 307–314,
- [20] R. Rajeswari and S. Kanmani, “A study on synergistic effect of photocatalytic ozonation for carbaryl degradation,” *Desalination*, vol. 242(1–3) (2009) 277–285.
- [21] Y. Chen, W. Huang, D. He, Y. Situ, and H. Huang, Construction of Heterostructured g-C₃N₄/Ag/TiO₂ Microspheres with Enhanced Photocatalysis

- Performance under Visible-Light Irradiation, *ACS Appl. Mater. Interfaces*, 6(16) (2014) 14405–14414.
- [22] M. Liu, S. Wei, W. Chen, L. Gao, X. Li, L. Mao, H. Dang. Construction of direct Z-scheme g-C₃N₄/TiO₂ nanorod composites for promoting photocatalytic activity. *J. Chin. Chem Soc.* (2019) 1–7.
- [23] M. Y. Yan, Z.Y. Jiang, J. M. Zheng, Y. M. Lin, Z. Y. Zhang. Theoretical study on transport-scheme conversion of g-C₃N₄/TiO₂ heterojunctions by oxygen vacancies. *Appl. Surf. Sci.* 531 (2020) 147318.
- [24] J. Wang, Q. Zhang, F. Deng, X. Luo, D.D. Dionysiou. Rapid toxicity elimination of organic pollutants by the photocatalysis of environment-friendly and magnetically recoverable step-scheme SnFe₂O₄/ZnFe₂O₄ nano-heterojunctions. *Chem. Eng. J.* 379 (2020) 122264.
- [25] J. Fu, Q. Xu, J. Low, C. Jiang, J. Yu, Ultrathin 2D/2D WO₃/g-C₃N₄ step-scheme H₂-production photocatalyst, *Appl. Catal. B Environ.*, 243 (2019) 556-565
- [26] Y. Wu, D. Mengb, Q. Guo, D. Gao, L. Wang. Study on TiO₂/g-C₃N₄ S-Scheme heterojunction photocatalyst for enhanced formaldehyde decomposition. *Optical Materials* (2022) 126, 112213.
- [27] Q. Xu, L. Zhang, B. Cheng, J. Fan, Jiaguo Yu. S-scheme heterojunction photocatalyst, *Chem* 6 (2020) 1543-1559.
- [28] Q., Xu, D. Ma, S. Yang, Z. Tian, B. Cheng, J.Fan. Novel g-C₃N₄/g-C₃N₄ S-scheme isotype heterojunction for improved photocatalytic hydrogen generation. *Appl. Surf. Sci.* (2019) 495, 143555.
- [29] M. H. Barzegar, M. M. Sabzehmeidani, M. Ghaedi, V. M. Avargani, Z. Moradi, V. A.L. Roy, H. Heidari. S-scheme heterojunction g-C₃N₄/TiO₂ with enhanced

- photocatalytic activity for degradation of a binary mixture of cationic dyes using solar parabolic trough reactor. *Chemical Engineering Research and Design* 174 (2021) 307–318.
- [30] B. Guo, B. Liu, C. Wang, Y. Wang, S. Yin, M. S. Javed, W. Han. S-scheme $\text{Ti}_{0.7}\text{Sn}_{0.3}\text{O}_2/\text{g-C}_3\text{N}_4$ heterojunction composite for enhanced photocatalytic pollutants degradation. *Journal of Environmental Chemical Engineering* 10 (2022) 107118.
- [31] V.H. Nguyen, S. A. Delbari, M. Mousavi, A. S. Namini, J. B. Ghasemi, Q. Van Le, Mehdi S. Asl, M. Mohammadi, M. Shokouhimehr. $\text{g-C}_3\text{N}_4$ -nanosheet/ ZnCr_2O_4 S-scheme heterojunction photocatalyst with enhanced visible-light photocatalytic activity for degradation of phenol and tetracycline. *Separation and Purification Technology* (2021) 118511.
- [32] R. Wang, J. Shen, W. Zhang, Q. Liu, M. Zhang, H. Tang Zulficar, Build-in electric field induced step-scheme $\text{TiO}_2/\text{W}_{18}\text{O}_{49}$ heterojunction for enhanced photocatalytic activity under visible-light irradiation, *Ceram. Int.* 46 (2020) 23–30.
- [33] J. Wang, G. Wang, B. Cheng, J. Yu, J. Fan. Sulfur-doped $\text{g-C}_3\text{N}_4/\text{TiO}_2$. S-scheme heterojunction photocatalyst for Congo Red photodegradation. *Chinese Journal of Catalysis* 42 (2021) 56–68.
- [34] Pharmacomedicale, Carbamazépine (sauf comme régulateur de l'humeur),” 2017. [Online]. Available: <https://pharmacomedicale.org/medicaments/par-specialites/item/carbamazepine>. [Accessed: 05-Sep-2018].
- [35] S. Wang and J. Wang, Carbamazepine degradation by gamma irradiation coupled to biological treatment, *J. Hazard. Mater.*, 321(2017) 639–646.

- [36] C. Pragathiswaran, C. Smitha, B. Mahin Abbubakkar, P. Govindhan, N. Anantha Krishnan, Synthesis and characterization of TiO₂/ZnO–Ag nanocomposite for photocatalytic degradation of dyes and anti-microbial activity, *Materials Today: Proceedings*, 45 (2) (2021) 3357-3364.
- [37] F. Li, Y. Huang, C. Gao, X. Wu, the enhanced photo-catalytic CO₂ reduction performance of g-C₃N₄ with high selectivity by coupling CoNiS_x, *Materials Research Bulletin*, 144 (2021) 111488.
- [38] X.-j. Wang, W.-y. Yang, F.-t. Li, Y.-b. Xue, R.-h. Liu, Y.-j. Hao, In situ micro wave assisted synthesis of porous N TiO₂/g-C₃N₄ heterojunctions with enhanced visiblelight photocatalytic properties, *Ind. Eng. Chem. Res.* 52 (2013) 17140–17150.
- [39] L.A. Al-Hajjia, Adel A. Ismaila,e, M. Faycal Atitarb, I. Abdelfattahc, Ahmed Mohamed El-Toni, Construction of mesoporous g-C₃N₄/TiO₂ nanocrystals with enhanced photonic efficiency, 45(1) (2019) 1265-1272.
- [40] Y. Li, R. Wang, H. Li, X. Wei, J. Feng, K. Liu, Y. Dang, A. Zhou, Efficient and Stable Photoelectrochemical Seawater Splitting with TiO₂@g-C₃N₄ Nanorod Arrays Decorated by Co-Pi, *J. Phys. Chem. C.* 119 (2015) 20283–20292.
- [41] Y. Liao, G. Wang, J. Wang, K. Wang, S. Yan, Y. Su, Nitrogen vacancy induced in situ g-C₃N₄ p-n homojunction for boosting visible light-driven hydrogen evolution, *Journal of Colloid and Interface Science* 587 (2021) 110–120.
- [42] Y. Liu, S. Wu, J. Liu, S. Xie, Y. Liu. Synthesis of g-C₃N₄/TiO₂ nanostructures for enhanced photocatalytic reduction of U(VI) in water. *RSC Adv.* 11 (2021) 4810.
- [43] N. Boonprakob, N. Wetchakun, S. Phanichphant, D. Waxler, P. Sherrell, A. Nattestad, J. Chen, B. Inceesungvorn. Enhanced visible-light photocatalytic activity of g-C₃N₄/TiO₂ films. *J. Colloid Interf. Sci.* 417 (2014) 402–409.

- [44] Y. Li, S. Wu, L. Huang, J. Wang, H. Xu, and H. Li, Synthesis of carbon-doped g-C₃N₄ composites with enhanced visible-light photocatalytic activity, *Mater. Lett.*, 137 (2014) 281–284,
- [45] M.A. Alcudia-Ramos, M.O. Fuentez-Torres, F. Ortiz-Chi, C.G. Espinosa-González, N. Hernández-Como, D.S. García-Zaleta, M.K. Kesarla, J.G. Torres-Torres, V. Collins-Martínez, S. Godavarthi, Fabrication of g-C₃N₄/TiO₂ heterojunction composite for enhanced photocatalytic hydrogen production, *Ceramics International*, 46 (1) (2020) 38-45.
- [46] R. Hao, G. Wang, H. Tang, L. Sun, C. Xu, D. Han, Template-free preparation of macro/mesoporous g-C₃N₄/TiO₂ heterojunction photocatalysts, with enhanced visible light photocatalytic activity, *Applied Catalysis B: Environmental*, 187 (2016) 47-58.
- [47] J. Li, Y. Liu, H. Li, C. Chen, Fabrication of g-C₃N₄/TiO₂ composite photocatalyst with extended absorption wavelength range and enhanced photocatalytic performance, *Journal of Photochemistry and Photobiology A: Chemistry*, 317 (2016) 151-160.
- [48] M. Anjum, R. Kumar, S.M. Abdelbasir, M.A. Barakat, Carbon nitride/titania nanotubes composite for photocatalytic degradation of organics in water and sludge: Pre-treatment of sludge, anaerobic digestion and biogas production, *Journal of Environmental Management*, 223 (2018) 495-502.
- [49] A. Toghan, H. M. Abd El-Lateef, K. K. Taha, A. Modwi, Mesoporous TiO₂@g-C₃N₄ composite: construction, characterization, and boosting indigo carmine dye destruction, *Diamond and Related Materials*, 118 (2021) 108491.
- [50] P. John, K. Johari, N. Gnanasundaram, A. Appusamy, M. Thanabalan, enhanced photocatalytic performance of visible light driven TiO₂/g-C₃N₄ for degradation of

- diclofenac in aqueous solution, *Environmental Technology & Innovation*, 22 (2021) 101412.
- [51] R.A. Senthil, J. Theerthagiri, A. Selvi, J. Madhavan. Synthesis and characterization of low-cost g-C₃N₄/TiO₂ composite with enhanced photocatalytic performance under visible-light irradiation. *Optical Mater.* 64 (2017) 533–539.
- [52] Y. Chen, W. Huang, D. He, Y. Situ, H. Huang, Construction of heterostructured g-C₃N₄/Ag/TiO₂ microspheres with enhanced photocatalysis performance under visible-light irradiation. *ACS Appl. Mater. Interfaces* 6 (2014) 14405–14414.
- [53] Y. Xu and MAA. Schoonen. The absolute energy positions of conduction and valence bands of selected semiconducting minerals. *Am. Mineral.* 85 (2000) 543.
- [54] J. Liu, B. Chenga, J. Yu. A new understanding of the photocatalytic mechanism of the direct Z-scheme g-C₃N₄/TiO₂ heterostructure. *Physical Chemistry, Chemical Physics* 18 (2016) 31175-31183.
- [55] L. Wang, Y. Dong, J. Zhang, F. Tao, J. Xu, Construction of NiO/g-C₃N₄ p-n heterojunctions for enhanced photocatalytic CO₂ reduction, *Journal of Solid State Chemistry*, Volume 308 (2022) 122878.
- [56] J. Li, Y. Yin, E. Liu, Y. Ma, J. Wan, J. Fan, X. Hu, In situ growing Bi₂MoO₆ on gC₃N₄ nanosheets with enhanced photocatalytic hydrogen evolution and disinfection of bacteria under visible light irradiation, *J. Hazard. Mater.* 321 (2017) 183–192.
- [57] H. Zeghioud, M. Kamagate, L. S. Coulibaly, S. Rtimi, A. A. Assadi, Photocatalytic degradation of binary and ternary mixtures of antibiotics: reactive species

investigation in pilot scale, *Chemical Engineering Research and Design*, 144 (2019) 300-309.

- [58] C. Sirtori, A. Zapata, S. Malato, W. Gernjak, A.R. Fernández-Alba, A. Agüera, Solar photocatalytic treatment of quinolones: intermediates and toxicity evaluation. *Photochem. Photobiol. Sci.* 8 (2009) 644–651.

Pre-proof